Structural Engineering and Mechanics, *Vol. 75, No. 4 (2020) 507-518*
DOI: https://doi.org/10.12989/sem.2020.75.4.507

Prediction and analysis of structural noise of a box girder using hybrid FE-SEA method

Wen-jun Luo[1a], Zi-zheng Zhang[1], Bao-you Wu[2], Chang-jie Xu[*1] and Peng-qi Yang[3]

[1] *MOE Engineering Research Center of Railway Environment Vibration and Noise, East China Jiaotong University, Nanchang Jiangxi province, China*
[2] *China Railway Electrification Engineering Group Company Limited, Wanshou South Side Jinjiacun No. 1, Fengtai District, Beijing, China*
[3] *JSTI Group Company Limited, Fuchunjiang East Street, No. 8, Jian'ou District, Nanjing, Jiangsu province, China*

(Received January 2, 2020, Revised February 16, 2020, Accepted February 22, 2020)

Abstract. With the rapid development of rail transit, rail transit noise needs to be paid more and more attention. In order to accurately and effectively analyze the characteristics of low-frequency noise, a prediction model of vibration of box girder was established based on the hybrid FE-SEA method. When the train speed is 140 km/h, 200 km/h and 250 km/h, the vibration and noise of the box girder induced by the vertical wheel-rail interaction in the frequency range of 20-500 Hz are analyzed. Detailed analysis of the energy level, sound pressure contribution, modal analysis and vibration loss power of each slab at the operating speed of 140 km /h. The results show that: (1) When the train runs at a speed of 140km/h, the roof contributes more to the sound pressure at the far sound field point. Analyzing the frequency range from 20 to 500 Hz: The top plate plays a very important role in controlling sound pressure, contributing up to 70% of the sound pressure at peak frequencies. (2) When the train is traveling at various speeds, the maximum amplitude of structural vibration and noise generated by the viaduct occurs at 50 Hz. The vibration acceleration of the box beam at the far field point and near field point is mainly concentrated in the frequency range of 31.5-100 Hz, which is consistent with the dominant frequency band of wheel-rail force. Therefore, the main frequency of reducing the vibration and noise of the box beam is 31.5-100 Hz. (3) The vibration energy level and sound pressure level of the box bridge at different speeds are basically the same. The laws of vibration energy and sound pressure follow the rules below: web <wing plate <top plate. (4) When the train is running at a higher speed, the noise and vibration of the bridge structure are larger. (5) The hybrid FE-SEA method is used to predict the structural noise of the box beam, which not only improves the efficiency, but also improves the calculation accuracy, thereby expanding the frequency range of the structural noise and improving the prediction accuracy.

Keywords: box-girder; local vibration; structural noise; hybrid FE-SEA method

1. Introduction

The noise of urban rail transit concrete bridges falls in the low frequency range, it is easy to pass through obstacles, such as walls, and it will reduce people's attention, reaction time and speech recognition ability (Ross *et al*. 2011, Luo *et al*. 2016). People's tolerance for low-frequency environmental noise is reduced (Bengtsson *et al*. 2003, Schulte-Warning *et al*. 2005). For future urban rail transit bridges, especially in densely populated areas, effective noise attenuation of concrete bridges must be guaranteed. Based on the literature review, further research should focus on the noise radiation and local vibration of this kind of structures. Generally, the noise problem of bridge structures is complicated and involves many interrelated research problems. It is very difficult to study the noise field of complex bridges using analytical methods. In recent years, a great deal of research has been conducted on the noise and vibration related to bridges. Ouelaa *et al*. (2005) considered vehicle mass, damping, and other factors, and then combined the vehicle-bridge coupled vibration equation with the derived bridge acoustic radiation wave equation to obtain the sound pressure of the bridge noise in the spatial sound field. Luo *et al*. (2015) selected solid elements and used the finite element method (FEM) to study the local vibration of high-speed railway viaduct box bridges in detail. Song *et al*.(2015) predicted the low frequency noise of a U-beam of rail transit concrete based on the 2.5-dimensional infinite element method. Compared with calculation results using the 3-dimensional boundary element method, the proposed method can quickly predict the structural noise of bridge without losing much accuracy. Gao *et al.* (2020) presents an improved hybrid FE-SEA method to overcome this problem. Liu *et al*. (2020) proposed several formulae for the bridge-borne noise in terms of the train speed and distance by using FE and SEA to model the concrete deck and steel stringer respectively. The vibration and noise of railway box girder were studied by using three-dimensional boundary element method and verified by testing (Zhang *et al*. 2016). Liu *et al*. (2015) used the railway bridge coupling vibration theory to study the vertical vibration of bridges and the contribution of components. Li *et al*. (2012) studied the vibration and noise of railway bridges by combining finite element and acoustic

*Corresponding author, Professor
E-mail: xucj@zju.edu.cn
[a] Professor
E-mail: lwj06051979@163.com

http://www.techno-press.com/journals/sem&subpage=7
ISSN: 1225-4568 (Print), 1598-6217 (Online)

computer programs. Zhang *et al*. (2013) conducted on numerical simulation and on-site measurement of low-frequency structural noise of concrete bridges. Song *et al*(2018) studied the spectral characteristics and spatial distribution laws of bridge radiated noise and rail radiated noise, and verified the accuracy of the numerical calculation method through actual comparison. Fang *et al*. (2013) studied the influence of the span of a simple beam, the stiffness under the rail, and the track structure on the bridge on the vibration transmission characteristics and noise radiation of the elevated bridge structure. Luo *et al*. (2017) studied the noise radiation characteristics directly below the subway elevated box girder in 0-50Hz. Luo *et al*. (2018) studied the spectral and spatial characteristics of the vibration and structural noise of U-beam in the frequency range of 1.25-500 Hz.

The noise is mainly distributed in the space under the box girder bridge; in the range of 80-630 Hz, the noise near the floor of the box girder predominates. Cui *et al*. (2015) combined the finite element method and boundary element method to study the noise reduction characteristics and damping characteristics of the damping rails of high-speed railways. Thompson *et al*. (2009) provided the noise level spectrum measured from a steel railway bridge. Peaks of the noise level spectrum at different speeds were recorded. Wang *et al*. (2014) studied the dynamic response of bridges with different paths at different speeds, and showed that the larger sound pressure level in the bridge structure was the substructure. Finite element method (FEM), boundary element method (BEM) and statistical energy analysis (SEA) are the main methods for studying the vibration and noise of bridge structures. FEM is suitable for the low and medium frequency range. However, it is not ideal for studying complex dynamic systems. The amount of BEM calculations increases rapidly with increasing degrees of freedom, especially when performing high-frequency analysis, which takes a lot of time. FEM and BEM are commonly used to study vibration and noise in the low frequency range (<200 Hz). For low frequency analysis, due to the lack of modal density in structural vibration, the accuracy of the SEA can be greatly reduced, so SEA is not suitable for low frequencies.

Based on the FE and hybrid FE-SEA methods, a prediction model for bridge vibration is established. The characteristics of local vibration and structural noise of the box beam induced by the vertical wheel-rail interaction in the frequency range of 20-500 Hz are analyzed. The vibration response of the flat plate, the sound pressure contribution, and the vibration power loss of the box beam were obtained. Compared with traditional methods, the hybrid FE-SEA method is more accurate.

2. Correlation theory and prediction model

2.1 The basic principle of hybrid FE-SEA method and the vibration prediction model

The hybrid FE-SEA method based on wave theory (Chen *et al*. 2011 and Shorter *et al*. 2005) treats the definite boundary of the physical body as a random boundary. According to different boundary conditions, the displacement field at the boundary is divided into direct field and reverberation field. In the hybrid FE-SEA model, the elastic wave is reflected on the coupling boundary between the FE subsystem (direct field) and the SEA subsystem (reverberation field), and the FE subsystem is subject to additional forces (reverberation force) in the reverb area of influence.

In analyzing the system structure vibration, the frequencies of the studied object can be divided into low, intermediate, and high frequency ranges according to the size of subsystem's bandwidth Δf defined by a N value (Li et *al* .2013). $N \leq 1$, $1 < N < 5$, and $N \geq 5$ represent the low, intermediate, and high frequency regions, respectively. For a mixed FE-SEA model, at the coupling boundary between the SEA and the FE subsystem, the elastic wave will produce a reflection effect, which will generate additional reverberation force to the FE subsystem. Therefore, the overall dynamic equation of the FE subsystem can be expressed as

$$D_{tot}q = f_{ext} + \sum_{k=1}^{N} f_{rev}^{(k)} \tag{1}$$

$$D_{tot} = D_d + \sum_{k=1}^{N} D_{dir}^{(k)} \tag{2}$$

In the above two formulas: N is the number of SEA subsystems; q is the degree of freedom vector of the FE subsystem; D_{tot} is the overall dynamic stiffness matrix of the FE subsystem; D_d is the dynamic stiffness matrix of the FE subsystem itself (from Its mass, stiffness and damping matrix are determined); *D(k) dir* represents the direct dynamic stiffness matrix generated by the kth SEA subsystem to the FE subsystem; f_{ext} represents the action on the FE subsystem *f(k) rev* represents the reverberation force vector generated by the k-th SEA subsystem on the coupling boundary.

From Equation (1), the degree of freedom q of the FE subsystem can be expressed as

$$q = D_{tot}^{-1} f_{ext} + \sum_{k=1}^{N} D_{tot}^{-1} f_{rev}^{(k)} \tag{3}$$

The reverberation force on the coupling boundary can be determined by

$$S_{ff,rev}^{(k)} = (\frac{4E_k}{\pi\omega n_k}) Im\left\{D_{dir}^{(k)}\right\} \tag{4}$$

where *S(k) ff,rev* is the cross-spectrum matrix of the reverberation force; E_k is the average vibration energy of the k-th SEA subsystem; n_k is the modal density of the k-th SEA subsystem; Im{}means taking the imaginary part; ω is the circle frequency. This formula establishes the relationship between the vibration energy of the SEA subsystem and the reverberation force on the coupling boundary, which is the key to the FE-SEA coupling theory.

According to the law of conservation of energy, the power balance equation of the FE-SEA coupling system can be expressed as

$$w(\eta_j+\eta_{d,j})E_j+\sum_{k=1}^{N} w\eta_{jk}n_j\left(\frac{E_j}{n_j}-\frac{E_k}{n_k}\right) = P_j+P_{ext,j}(j=1,2,\ldots,N) \quad (5)$$

where

$$w\eta_{d,j} = \left(\frac{2}{\pi n_j}\right)\sum_{r,s} Im\left\{D_{d\ ,\ rs}\right\}(D_{tot}^{-1}\, Im\left\{D_{dir}^{(j)}\right\} D_{tot}^{-1*T})_{rs} \quad (6)$$

$$w\eta_{jk}n_j=\left(\frac{2}{\pi}\right)\sum_{r,s} Im\left\{D_{dir,rs}^{(j)}\right\}(D_{tot}^{-1}\, Im\left\{D_{dir}^{(k)}\right\} D_{tot}^{-1*T})_{rs} \quad (7)$$

$$P_{ext,j}=\left(\frac{w}{2}\right)\sum_{r,s} Im\left\{D_{dir,rs}^{(j)}\right\}(D_{tot}^{-1}S_{ff}D_{tot}^{-1*T})_{rs} \quad (8)$$

where η_j is the internal loss factor of the j-th SEA subsystem; η_j is the additional loss factor generated by the FE subsystem to the j-th SEA subsystem; η_{jk} is the SEA subsystem The coupling loss factor between j and the SEA subsystem; P_j is the external input power directly applied to the j-th SEA subsystem; $P_{ext,j}$ is the external excitation pair applied to the j-th subsystem Input power generated by the SEA subsystem.

All of the symbols which appear in Eqs. (5)–(8) have been previously defined, apart from n_j, the loss factor of subsystem j, and P_j, which represents the power input to subsystem j arising from forces applied directly to the subsystem (in contrast to P_{ext} , which arises from forces applied to the deterministic system). The complete response of the system is found by solving Eq. (5) to yield the subsystem energies, following which Eq. (9) is used to yield the response of the deterministic system

According to equations (3) to (4), the cross-spectrum matrix of degrees of freedom q of the FE subsystem can be obtained.

$$S_{qq}=D_{tot}^{-1}\left[S_{ff,ext}+\sum_{k=1}^{N}\left(\frac{4E_k}{\pi w n_k}\right) Im\left\{D_{dir}^{(k)}\right\}\right]D_{tot}^{-1*T} \quad (9)$$

In the formula, $S_{ff,ext}$ represents the external excitation cross-spectrum matrix acting on the FE subsystem; the superscripts "*" and "T" represent conjugate operation and transpose operation, respectively.

It can be noted that Eqs. (5) and (9) relate to the response of the system at a particular frequency o, and all of the averaging involved relates to ensemble averaging rather than averaging across a frequency band.

The average vibration energy of each SEA subsystem can be obtained from formula (5), and the degrees of freedom of the FE subsystem can be obtained from formula (9), and then physical quantities such as the vibration speed and acceleration of the FE subsystem can be obtained. On this basis, through the theory of noise radiation, the sound pressure propagating to any point in space can be obtained.

Taking the box girder as an example, the local vibration model is analyzed by the FE-SEA hybrid method. The vibration frequency for the box girder is 20-500 Hz, as determined from the acoustic radiation analysis. For calculation precision and efficiency, plate elements are used. According to whether the bending modulus of each slab is greater than 5, the box girder model is established in different bands. The relation between the bending modal density and the frequency of the beam under wheel-rail forces is shown Fig.1. According to whether the bending mode density is greater than 5, the frequency division segment modeling is carried out (Han *et al.*2012, Lei *et al.*2004). In the low frequency domain of 20-160 Hz, all box girder plates are not satisfied with the requirement of establishing the SEA model. So, the whole FE structure needs to be established in this frequency domain. The unit length is unified as 0.2 m, which satisfies the requirement of precision. In the frequency domain of 160-315 Hz, the flexural modal density of the wing plate is less than 5. So, the FE subsystem is established, while the web slab, the top slab, and the bottom slab remain as SEA subsystems. In the frequency domain of 315-500 Hz, the mode number of each slab is more than 5. So, it is built as a SEA subsystem. The

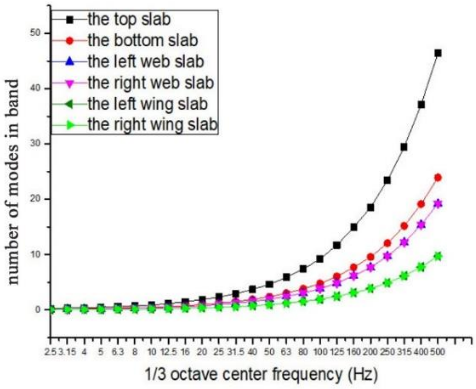

Fig. 1 Relationship between the bending mode density and the frequency of each section of box-girder

Table 1 The classification of subsystems

Frequency band (Hz)	Subsystem type	Plate name
20~160	FE	the top slab、the bottom slab、the left (right) web slab、the left (right) wing slab
	SEA	\
160~315	FE	the left (right) wing slab
	SEA	the bottom slab、the left (right) web slab、the top slab
315~500	FE	\
	SEA	the bottom slab、the left (right) web slab、the left (right) wing slab b、the top slab

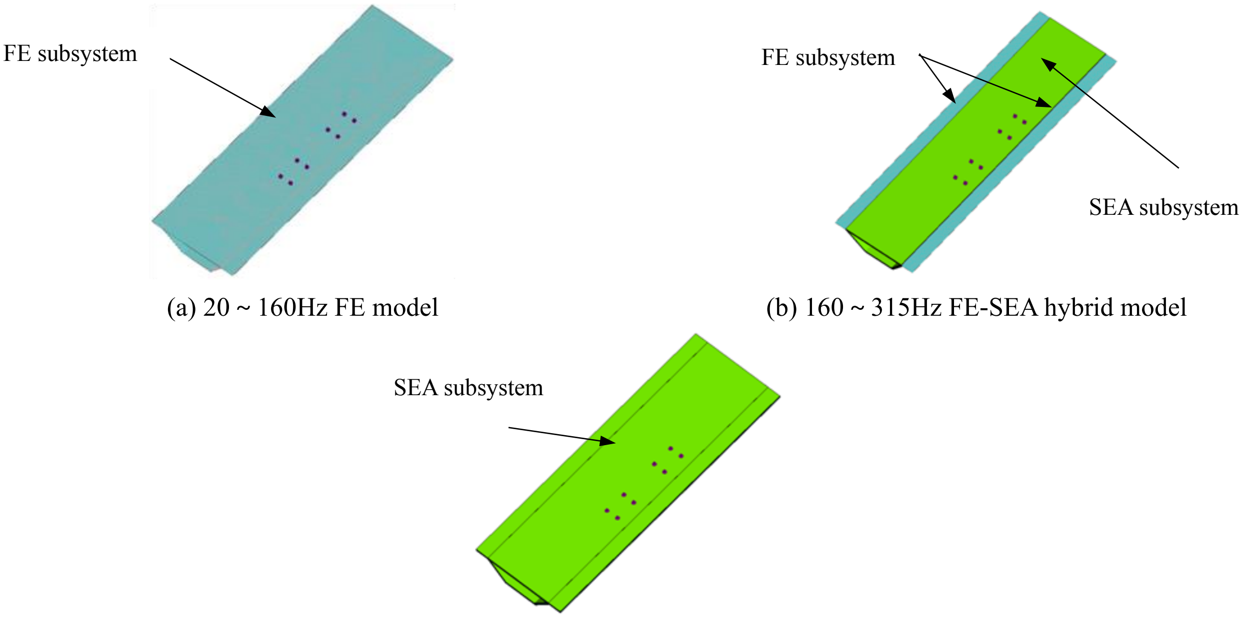

(a) 20 ~ 160Hz FE model (b) 160 ~ 315Hz FE-SEA hybrid model

(c) 315 ~ 500Hz SEA model

Fig. 2 The box-girder mode

frequency of vibration and acoustic radiation of the box girder is 20-500 Hz and slab and shell type units are used. Different frequency band box girder model is shown in Fig.2. The subsystem classification for each slab in different frequency bands is shown in Table 1.

2.2 Sound radiation of the bridge structure

A system consisting of multiple rectangular plates (subsystems) can be considered as a box beam structure. Each rectangular plate has a width of a and a length of b. The radiated sound power can be expressed as(Zhang *et al*.2016 and Langley *et al* 2009)

$$W_i = \rho_a c_a \sigma_i S_i \langle \overline{V}_i^2 \rangle \tag{10}$$

In the above formula : the ρ_a is the air density(kg/m^3), c_a is the noise velocity in the air (m/s), σ_i is the radiation efficiency of the i-th subsystem, S_i is the superficial area of the i-th subsystem (m/s^2), and$\langle \overline{V}_i^2 \rangle$ is mean square value of the velocity((m/s) ^{2}). Assume that the vertical distance from the center of the rectangular plate to the point M is r. When $r \le a/\pi$, the noise source emits a plane wave, and its amplitude does not decay with the distance traveled. The root mean square value of the sound pressure radiated from the i-th subsystem at the point M is:

$$\langle \bar{p}_i^2 \rangle_M = \frac{\pi \rho_a c_a W_i}{4ab} \tag{11}$$

When $b/\pi > r > a/\pi$, the noise source can be simplified as an infinite line noise source, then:

$$\langle \bar{p}_i^2 \rangle_M = \frac{\pi \rho_a c_a W_i}{4br} \tag{12}$$

When $r \ge b/\pi$, the noise source can be approximated as a point noise source,

$$\langle \bar{p}_i^2 \rangle_M = \frac{\pi \rho_a c_a W_i}{4\pi r^2} \tag{13}$$

Therefore, in the far field, the total sound pressure of the box girder at point M can be obtained by the linear superposition principle.

In order to analyze the contribution of the vibration of each plate to the total sound pressure at a certain point, the sound pressure contribution coefficient D_c was introduced

$$D_c = Re * (\boldsymbol{p}_c \boldsymbol{p}^* / |\boldsymbol{p}|^2) \tag{14}$$

In the above formula: Re is the real part of a complex number, $\boldsymbol{P}$ is the total sound pressure at a certain point, $\boldsymbol{P}^*$ is the conjugate of $\boldsymbol{P}$, and $\boldsymbol{P}_c$ is the sound pressure radiated from each subsystem at a specific point.

2.3 Simulation analysis process

The simulation process is shown in Fig.3. First, through the SIMPACK rail coupling model, the time domain vertical wheel force signal is determined. Then, after the fast Fourier transform (FFT) analysis and 1/3 octave conversion by MATLAB, the equivalent wheel-rail interaction forces corresponding to the center frequencies of the 1/3 octave bands can be obtained. Depending on whether the modal density of each slab of the box girder is greater than 5, the FE and FE-SEA bridge model is set up. In the most unfavorable form, the wheel-rail force in the frequency domain is applied at the middle position of the bridge according to the wheelbase and vehicle distance, and the vibration response of the box girder is obtained. On this basis, the structural noise and vibration energy of the box girder are predicted and analyzed.

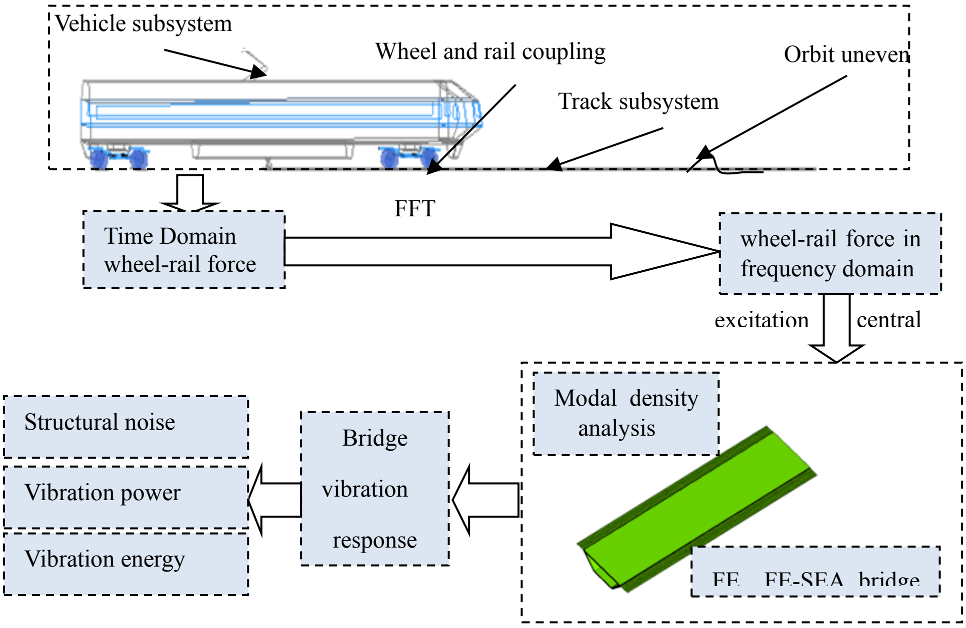

Fig. 3 Simulation flowchart of vibration and noise of box-girder structure

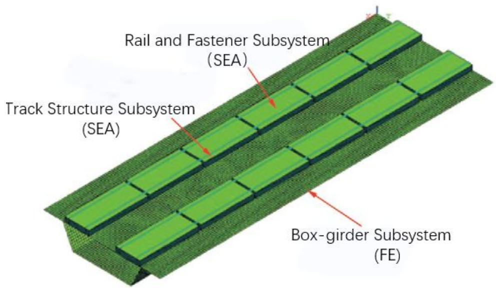

Fig. 4 FE-SEA model of the box-girder

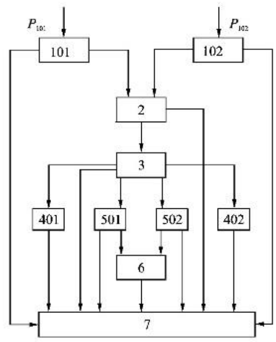

Fig. 5 Schematic diagram of power flow between sub-systems

The FE-SEA calculation model shown in Fig. 4 is established, which mainly includes the box girder subsystem, the rail subsystem and the track structure subsystem. Since the structural sound radiation comes from the bending vibration of the plate, the box beam is not considered in this study. For in-plane vibration of a plate, only out-of-plane bending vibration is considered. Figure 5 shows a schematic diagram of power flow transfer between subsystems. The boxes in the figure represent subsystems, and the connections between the subsystems represent power flow transfer. P_{101} and P_{102} are system input powers, which represent the input power of the two rails on the driving side by the wheel-rail interaction force; subsystem 7 is a virtual external space subsystem.

3. Model and related parameters

3.1 Vehicle-rail coupling model

The CRH2 vehicle rail coupling model is established by SIMPACK software, as shown in Fig.6. The track irregularity adopts the German high disturbance roughness spectrum. The train speed is about 140 km/h. By defining the geometric relationship of wheel-rail contact, the hinge of subsystem, and the setting of force elements and other parameters, the time-domain wheel-rail coupling vertical interaction force is obtained. The bogie is hinged with six degrees of freedom and the body is hinged with five degrees of freedom. The rail type is UIC60 and the wheel-rail contact is single-constraint. In order to accurately describe the wheel-rail contact relationship, the track, wheel reference, wheel profile reference, rail profile reference, wheel contact, and rail contact are introduced in the wheel-rail model to describe the relative movement between each rigid body of the rail and vehicle. After the FFT analysis and 1/3 octave conversion, the effective wheel-rail interaction forces corresponding the center frequencies of the 1/3 octave bands can be obtained. As shown in Fig.7, the maximum-amplitude frequency of the wheel-rail interaction force is 50 Hz.

3.2 Calculation model for the box bridge

A 32 m single-line simply supported box girder on a rail transit is established by the VA-one software (Zhang *et al*.

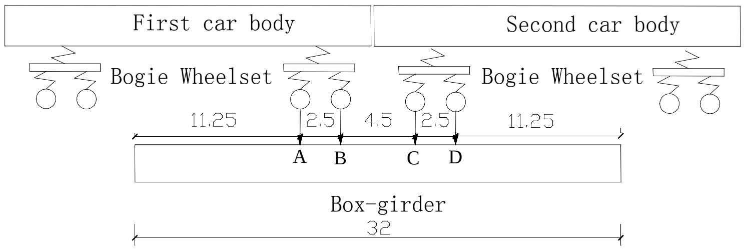

Fig. 6 Train-ballastless track-bridge coupling system

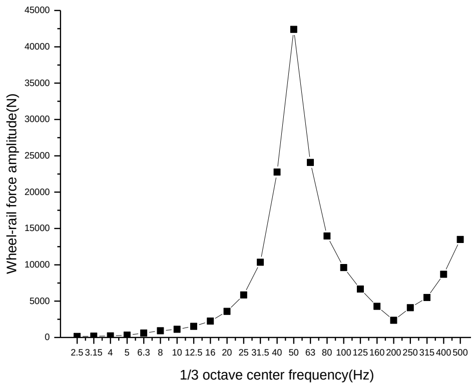

Fig. 7 Spectrum of wheel-rail interaction forces

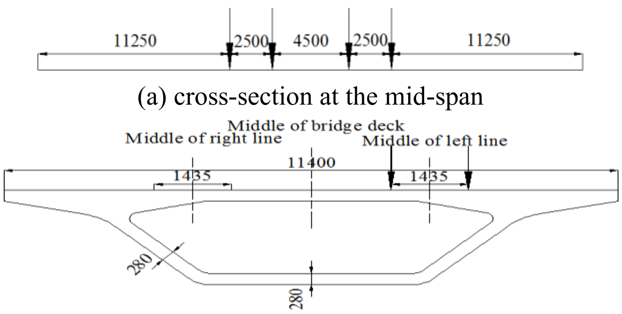

(b) Wind direction profile load locations (unit: mm)

Fig. 8 Bridge dimensions and load locations

2015). The thickness for the wing, web, and bottom slab of the box girder is 0.28 m. The bridge height is 2.354 m. The width of the bottom slab is about 3.946 m, and the arc between left and right webs has no difference. The simply supported boundary condition is simulated using a point constraint. Bridge dimensions and load locations are shown in Fig.8. The bogie wheelbase of the CRH2 type car is 2.5 m and the minimum track is 4.5 m between the adjacent carriages. The most disadvantageous loading condition with two car compartment joints at the middle of the bridge is considered. Relevant parameters for the bridge and vehicle are shown in Table 2 and Table 3 respectively.

Table 2 The structure parameters of box bridge

Parameters	Values	Parameters	Values
mass density (kg/m^3)	2650	The Poisson ratio	0.2
The elastic modulus (GPa)	34.5	loss factor	0.04
The shear modulus (GPa)	14.38	concrete grade	C55

Table 3 The structure parameters of A-type vehicle

Parameters	Values	Parameters	Values
Full quality (t)	51	The secondary spring stiffness(N/m)	1.9×10^5
Frame quality (t)	2.6	The secondary damping（kN*s/m）	40
Wheel set quality(t)	2.1	The fixed axle spacing(m)	2.5
The wheel distance between adjacent carriages (m)	4.5		

Table 4 The track parameters

Component	Parameters	Values
Rail	Elastic Modulus (Pa)	2.1×10^{11}
	Density (km/m^3)	7830
	Sectional area (cm^2)	77.45
	Poisson's ratio	0.3
Fastener	Stiffness(N/m)	9×10^7
	Damping(N·s/m)	6×10^4
Sleeper	Elastic Modulus (Pa)	3.5×10^{10}
	Density (km/m^3)	2600
	Poisson's ratio	0.22
Track bed	Elastic Modulus (Pa)	1.8×10^8
	Density (km/m^3)	1650
	Thickness (m)	0.6
	Poisson's ratio (m)	0.27

4. Analysis of vibration effects of the box bridge

4.1 Vibration response analysis

Using the box bridge model, the vertical acceleration levels of each plate at the midpoint of the box bridge beam were obtained, as shown in Fig.9. In the range of 20-500 Hz, the vibration of the left web slab is almost identical to the right one. The vibration for the left and right wing slab is virtually the same. The central spectrum of the 1/3 octave bands of each slab has peaks at 20 Hz and 50 Hz, as related to the local vibration of the box bridge. In general, the local vibration is larger than the global one and the maximum

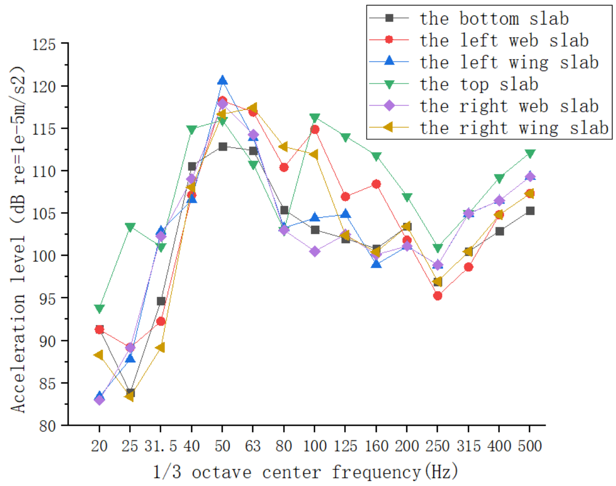

Fig. 9 The vertical acceleration levels of each plate at the mid box bridge section (140 km/h)

acceleration frequency is 50 Hz for each slab, matching with the frequency of the maximum wheel-rail force. The maximum acceleration levels at the midpoint are 120.6 dB, 117.9 dB, 118.3 dB, 116.9 dB, 113 dB, and 116 dB respectively for the left slab, right slab, left web slab, right web slab, bottom slab, and top slab. Within the range of 20-500 Hz, the dominant acceleration frequency level is around 40-80 Hz. This frequency range should be viewed as the key vibration reduction frequency band. Below 50 Hz, the acceleration at the top panel is the largest. The maximum acceleration in the frequency range of 50-500 Hz appears on the left wing slab because the wing slab is narrow and thin and the load is acting on the left slab. As shown in Fig.9, in the frequency range of 20-50 Hz, the vibration acceleration level of each slab peaks in 20Hz, and 50 Hz, considered as the main vibration attenuation bands. Below 40 Hz, the roof plays a major role in vibration and acts as a main vibration damping source. In the frequency range of 100-200Hz, the vibration acceleration levels of the left and right webs and the top slab are higher than those of the remaining panels. Hence, the vibration reduction measures should be taken in this frequency band for the left and right webs and the top slab. In the 200-500 Hz frequency band, the vibration acceleration level for each slab gradually increases with the left and right wings and the top slab more obviously, which can then be deemed as the main damping sources.

4.2 Model verification

In order to verify the correctness of the box bridge model, a field test under the same working condition was carried out. The speed of the vehicle is 140 km/h and the measured maximum vertical acceleration level the middle top slab is 112.9 dB. The calculated value is 111.5 dB, which is in good agreement with the measured value. For global vibration of the box bridge, the effects of track, cushion, pier, and the vibration damping between the components are usually ignored, and the orbit irregularity wavelength range of the theoretical simulation is not fully

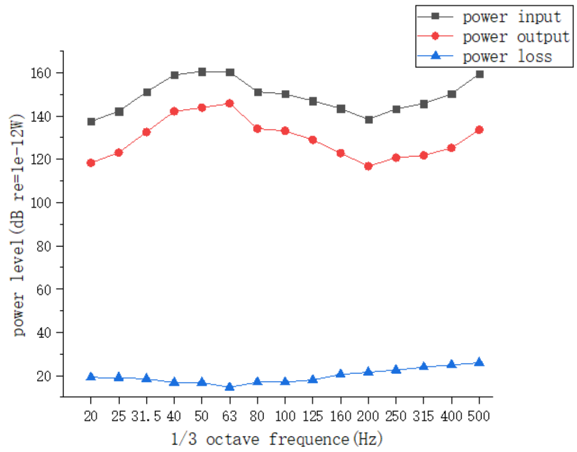

Fig. 10 Vibration power level loss of the box bridge

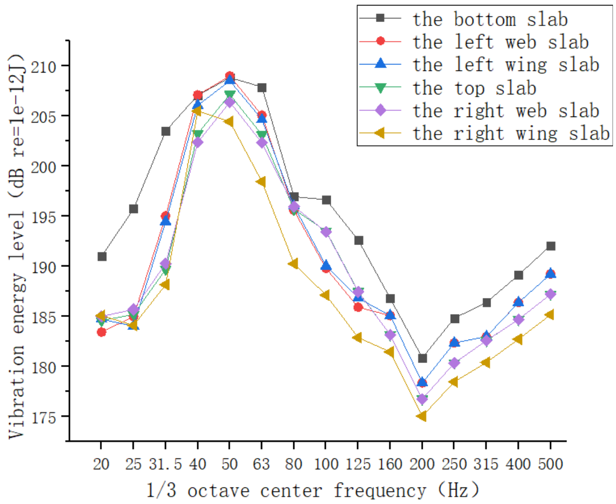

Fig. 11 Vibration energy level of the box bridge

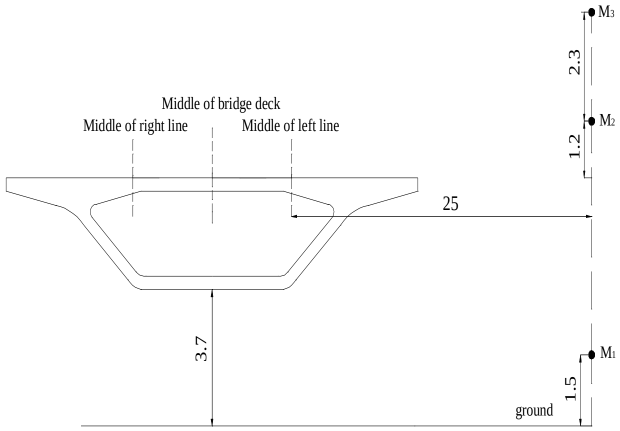

Fig. 12 Far field position (unit: m)

considered. The numerically simulated sound pressure in the 25 m far field is higher compared with the measured values. The comparison between the bridge vibration and the measured sound pressure level in the far field verifies the reliability of this model. Luo *et al*. (2019) how that the model is accurate and predictive and improves the calculation efficiency, and this method has high speed efficiency and accuracy.

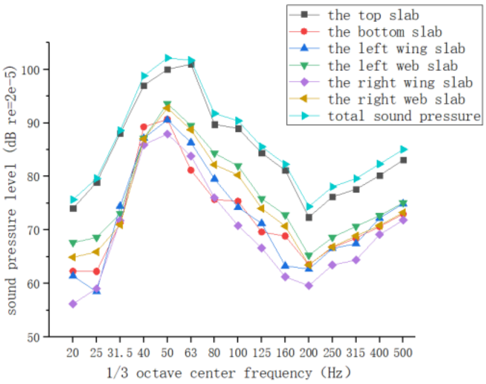

(a) M1

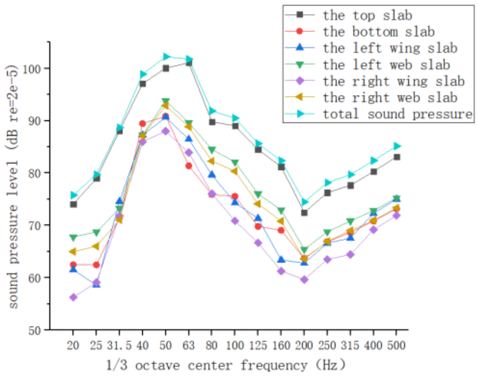

(b) M2

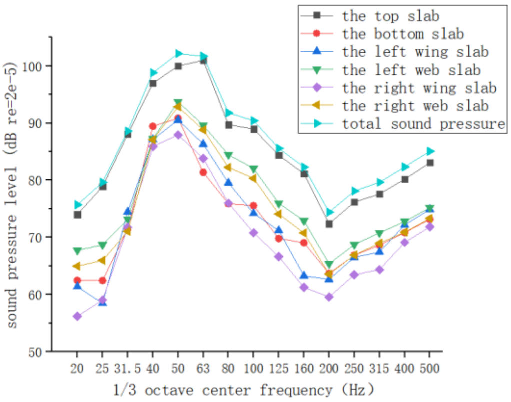

(c) M3

Fig. 13 Sound pressure levels due to the whole bridge and each plate at points M1, M2 and M3

4.3 Vibration power and energy analysis

The vibration power loss of the box bridge was obtained, as shown in Fig.10. The vibration loss of the box bridge is observed in the whole frequency range of 20-500 Hz. The power level loss in the frequency domain of 20-63 Hz is within the range of 18.4-19.2 dB and the vibration loss power increases gradually above 63 Hz. The vibration energy level of the box bridge was also obtained, as shown in Fig.12. Figure 11 shows that the plate vibration energy level characteristics are consistent with the law of sound pressure levels.

4.4 Arrangement of sound field points

To study the acoustic radiation of the structure, the sound pressure levels of each slab in the near-field zone (0.3 m away the central surface of each plate) were analyzed.

To study the acoustic radiation of the structure in the far-field zone, inspection points M1-M3 were set at the mid-span, as shown in Fig.11. M2 and M3 are 3.5 m and 1.2 m above the rail surface respectively and M1 is 1.5 m above the ground. They are all 25 m off the center of the left track line horizontally (Fig.12).

4.5 Sound pressure contribution

By analyzing the contribution of sound pressures of each slab of the box girder, an accurate noise reduction program may be proposed. The sound pressure levels due to the whole bridge and each plate at points M1-M3 are shown in Fig.13.

Taking M2 as an example, the sound contribution of each plate to M2 is shown in Fig.13(2). It can be seen that the overall sound pressure level peak center frequency of field M2 is at 50 Hz. The contribution of the top plate to M2 is the largest, followed by the left web and the right wing slab.

4.6 Modal analysis

The modal analysis of the box bridge is shown in Fig.14. From the figure, the local vibration is found in the modes of bridge which are symmetrical and antisymmetric.

5. Analysis of different speeds on the vibration and structural noises of box bridge

5.1 Analysis of structural noise

Trains were studied at speeds of 140 km/h, 200 km/h and 250 km/h respectively. Figure 15 shows that the acoustic pressure trends of all bridge slabs are basically the same in the near-field zone (0.3 m from the center surface). The acoustic pressure of the bridge peaks at 50 Hz. With increasing train speeds, the peak frequency of the sound

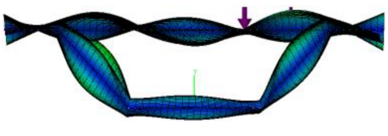

(a)50Hz

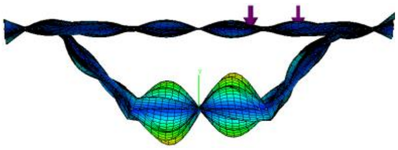

(b)200Hz

Fig. 14 Vibration modes of the box bridge

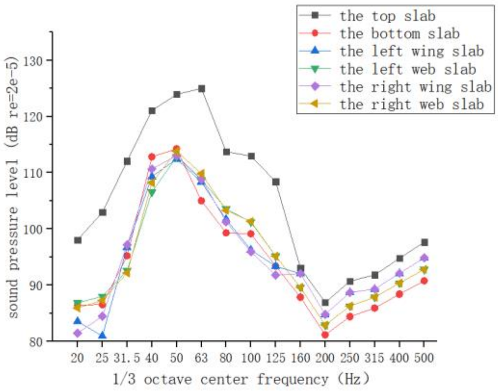

(a) 140km/h

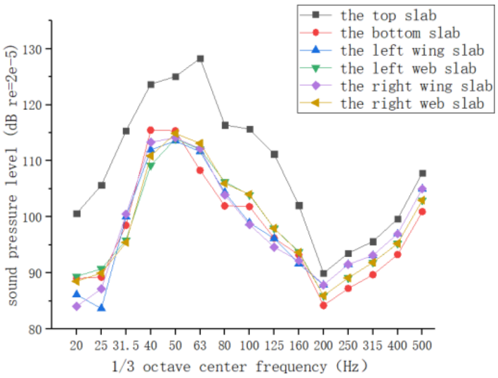

(b) 200km/h

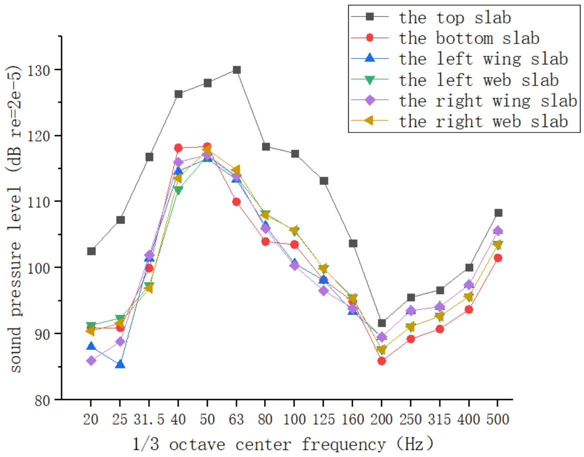

(c)250km/h

Fig. 15 Sound pressure levels of each slab in the near-field zone (0.3 m from the center surface)

pressure level for each slab increases and there is a significant peak at about 50Hz. At the same time, the acoustic pressure value of the top slab is dominant. The acoustic pressure value of the top plate dominates, and it can be concluded that the noise of the bridge body mainly comes from the top slab, which is mainly caused by the load on the top slab. When the speed of the train is 140 km/h, 200 km/h and 250 km/h respectively, the maximum value of the beam top slab is 125.0 dB, 125.1 dB, and 128.0dB. It can be seen that when the train is running at high speed, the speed changes have a greater impact on the sound pressure. In addition to the top slab, the sound pressure levels of the boards in the 20-500 Hz band are not much different. In the band of 200-500 Hz, the sound pressure level of the bottom slab is the smallest. Within 100-500 Hz frequency band, the sound pressure level around the wing is almost the same. This is because the left and right wing slabs are narrow and thin. At low frequencies, the structure near the excitation side produces a larger sound pressure. Due to the symmetry of the structure, the induced sound pressures at high frequencies are nearly uniform.

Three far-field sound pressures were obtained, as shown in Fig.16. It can be seen that there is almost no change in sound pressures at various measurement points. However, as the speed increases, the sound pressure at the three points outside the field increases and the maximum value is 102.0 dB, 103.0 dB and 106.0 dB respectively. This once again verifies that when the train is driving at high speed, the speed changes have a greater impact on the sound pressure.

5.2 Analysis of structural vibration response

As shown in Fig.17, when the train travels at different speeds, the vertical acceleration level trend of the bridges is basically consistent. The highest peak occurs at 50 Hz. As the speed increases, the acceleration level of the bridge increases. In the whole frequency band, the acceleration level of the top slab is relatively large, but the maximum

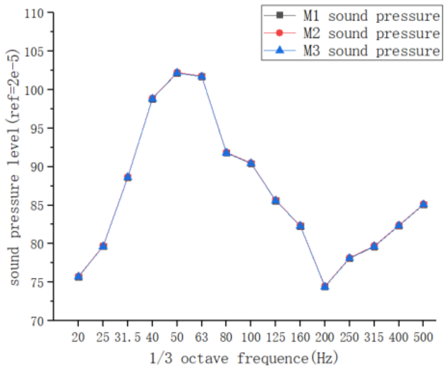

(a) 140km/h

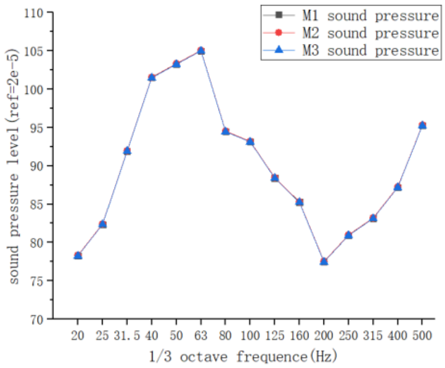

(b) 200km/h

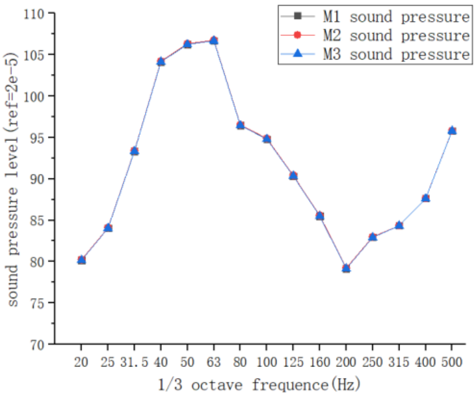

(c)250km/h

Fig. 16 Sound pressure level due to each slab in the near-field zone (M1, M2, M3)

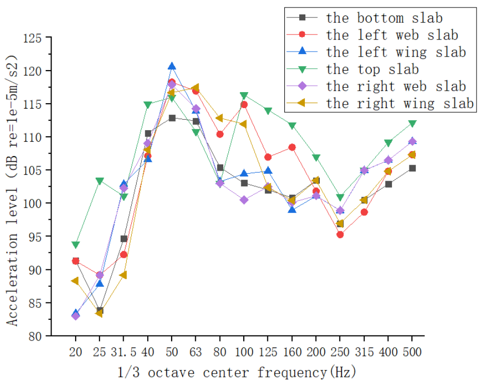

(a) 140km/h

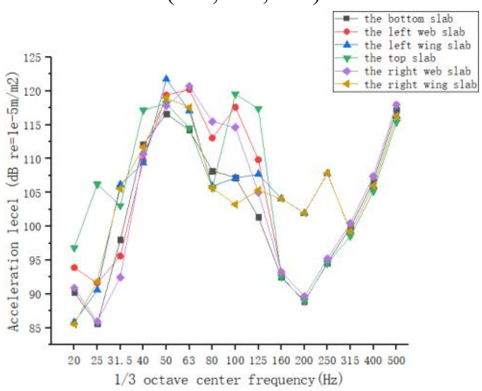

(b) 200km/h

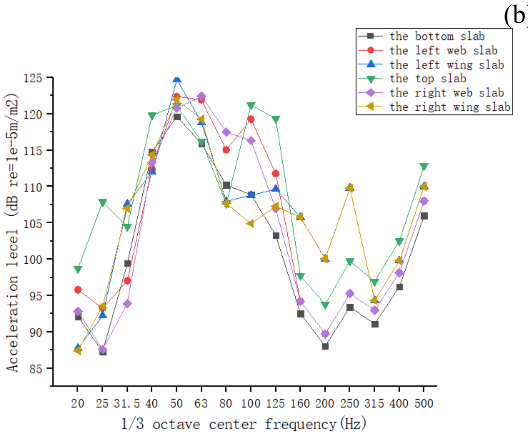

(c)250km/h

Fig. 17 The vertical acceleration levels of each slab at the mid box bridge section value of the acceleration level appears on the left wing slab. This is due to the fact that the wing slab is small in size and close to the load.

6. Conclusions

In this paper, the vibration simulation model of the rail transit box bridge structure under the vertical wheel-rail force is established by using the FE and the hybrid FE-SEA method. The vibration and noise of the railway box bridge in the 20-500 Hz band are carried out. The model is divided into FE and SEA subsystems according to the modal density of the local vibration of each slab of the box bridge. Based on this study, the following findings are summarized:

- The hybrid FE-SEA method takes advantages of finite element and statistical energy analysis, and can be modeled by using finite element or statistical energy analysis techniques for different characteristics of the subsystem. It can avoid the shortcomings of the time-consuming calculation of the deterministic FE method at high frequency and the poor precision of the SEA at low frequency, and solve the contradiction between the calculation efficiency and precision. The research results extend the frequency range of analyzing the local vibration of the box bridge and improve the prediction accuracy and calculation efficiency of the bridge structure vibration and structural noise spectrum characteristics.
- Taking the train speed of 140 km/h as an example, the top slab has the largest contribution to the sound pressure level of the near-field and far-field structure noise sound pressure level, and plays a major control role in the entire analysis frequency band. Therefore, the vibration reduction and noise reduction of the box bridge should mainly start from the top slab. The loss of the vibration power level is about 12.9-18.4 dB. The maximum amplitude frequency of vibration energy of box girder is 50 Hz, and the vibration energy level of each slab is the top slab> the wing slab >the web slab.
- When the train runs at speeds of 140 km/h, 200 km/h and 250 km/h, the vibration and noise generated by the bridge structure have almost the same regularity. The box bridge has the largest vibration response amplitude around 50 Hz, and the acceleration dominant frequency is concentrated at 50 Hz. In the entire 20-500 Hz band, the vibration of the top plate is larger than that of the other slabs, but the maximum vibration is at the left wing slab.
- When the train runs at different speeds, although the vibration of the top slab is greater than that of the other slabs, the sound p1ressure effect generated by the top slab is significantly greater than that of the other slabs. It can be concluded that the vibration of the bridge body is not necessarily related to the sound pressure generated.
- Under the effect of wheel-rail force, the maximum amplitude frequency of structural noise is 50 Hz, which is the same as the dominant frequency of the wheel-rail force and the maximum amplitude. Therefore, the main vibration-damping and noise-reducing frequency band of the box bridge should be the dominant frequency band of the wheel-rail force acting on it.

Acknowledgements

This research is supported by the National Natural Science Foundation (51768022, 51978265), Jiangxi Provincial Science and Technology Innovation Team Construction Plan (20181BCB24011), Jiangxi Provincial Academic and Technical Leader Training Program (20194BCJ22009), and the National Science Fund for Distinguished Young Scholars (51725802), to which the authors are very grateful.

References

Bengtsson, J., Persson, W.K. and Kjellberg A. (2003), "Evaluations of effects due to low-frequency noise in a low demanding work situation", *J. Sound Vib.*, **278**, 83-99. https://doi.org/10.1016/j.jsv.2003.09.061.

Chen, S.M., Wang, D.F. and Zan, J.M. (2011). "Interior noise prediction of the automobile based on hybrid FE-SEA Method", *Math. Problems in Eng.,* https://doi.org/10.1155/201 1/327170.

Cui, R., Gao, L. and Cai, X. (2015), "Research on damping and noise reduction characteristics of high-speed railway damping rails", *J. China Railway Soc..*, **37**(02), 78-84. https://doi.org/10.3969/j.issn.1001-8360.2015.02.012.

Fang, X., Gu, A. and Wu, J. (2013), "Analysis of vibration transfer characteristics of simple supported box girder bridges", *Urban Rapid Rail Transit.*, **26**(03), 84-88. https://doi.org/10.3969/j.issn.1672-6073.2013.03.022.

Gao, R., Zhang, Y. and Kennedy, D. (2020), "Application of the dynamic condensation approach to the hybrid FE-SEA model of mid-frequency vibration in complex built-up systems", *Comput. Struct.,* **228**. https://doi.org/10.1016/j.compstruc.2019.106156.

Han, J., Wu, D. and Li, Q. (2012), "Influence of deck thickness and stiffeners on structure-borne noise of the trough beams", *J. Vib. Eng.*, **2012**(5), 589-594. https://doi.org/10.16385/j.cnki.issn.1004-4523.2012.05.003.

Langley, R. and Cordioli, A. (2009), "Hybrid deterministic-statistical analysis of vibro-acoustic systems with domain couplings on statistical components", *J. Sound Vib.*, **32**1(3-5), 893-912. https://doi.org/10.1016/j.jsv.2008.10.007.

Langley, R.S. and Cordioli, J.A. (2009), "Hybrid deterministic-statistical analysis of vibroacoustic systems with domain couplings on statistical components", *J. Sound Vib.,* **321**(3-5), 893-912. https://doi.org/10.1016/j.jsv.2008.10.007.

Lei, X. and Sheng, X. (2004), *Railway Traffic Noise and Vibration*, Science Press, Beijing, China.

Li, J., Zhang, N. and Zhang, L. (2012), "Numerical simulation of vibration and structural noise of elevated bridges", *Environ. Eng.*, **S1**, 156-160. https://doi.org/10.13205/j.hjgc.2012.s1.008.

Li, X., Zhang, X., Liu, Q., Zhang, Z. and Li, Y. (2013), "Study on the full band predictio of bridge structure noise in high speed railway (I): theoretical model", *J. China Railway Soc.*, **35**(1), 101-107. https://doi.org/10.3969/j.issn.1001-8360.2013.01.016.

Liu, L., Fu, Q., Shao, W. and Li, J. (2015), "Analysis of panel acoustic contribution to box bridge structure", *J. Railway Sci. Eng.*, **12**(04), 743-748. https://doi.org/10.19713/j.cnki.43-1423/u.2015.04.005.

Liu, Q., Thompson, D., Xu, P., Feng, Q. and Li, X (2020), "Investigation of train-induced vibration and noise from a steel-concrete composite railway bridge using a hybrid finite element-statistical energy analysis method", *J. Sound Vib.*, **471**, 115-197. https://doi.org/10.1016/j.jsv.2020.115197.

Luo, W. and Cheng, L. (2016), "Vibration and noise analysis of single track U-Beam in urban rail transit", *J. Railway Eng.,* **34** (05), 89-93. https://doi.org/10.3969/j.issn.1006-2106.2017.05.016.

Luo, W. and Cheng, L. (2018), “Prediction and Analysis of Structural Noise from a U-beam Using the FE-SEA Hybrid Method”, *Prome-Traffic Transport.*, **30**(3), 333-342. https://doi.org/10.7307/ptt.v30i3.2721.

Luo, W. and Zhang, X. (2015), “Finite element analysis of local vibration of high speed railway viaduct”, *Noise Vib. Control*, **34**(06), 148-152. https://doi.org/10.3969/j.issn.1006-2106.2015.11.011.

Luo, W., Yang, P. and Zhang, Z. (2019), “Prediction and Analysis of Structural Noise of Box Girder Based on FE-SEA Hybrid Method”, *J. China Railway Soc.*, **08**, 100-107. https://doi.org/10.3969/j.issn.1001-8360.2019.08.013.

Luo, Y., Tang, J. and Lin, P. (2017), “Experimental analysis of noise radiation characteristics directly underneath an elevated box girder of subway”, *Sichuan Environ.*, **36**(03), 101-105. https://doi.org/10.14034/j.cnki.schj.2017.03.016.

Ouelaa, N., Rezaiguia, A. and Laulagnet, B. (2005), “Vibro-acoustic modelling of a railway bridge crossed by a train”, *Appl. Acoustics.*, **67**(5), 461-475. https://doi.org/10.1016/j.apacoust.2005.07.005.

Ross, Z., Kheirbek, I., Clougherty, J.E., Ito, K., Matte, T., Markowitz, S. and Eisl, H. (2011), “Noise, air pollutants and traffic: continuous measurement and correlation at a high-traffic location in New York City”, *Environ. Res..*, **2011**(111), 1054-1063. https://doi.org/10.1016/j.envres.2011.09.004.

Schulte-Warning, B., Beier, M., Degen, K.G. and Stiebel, D. (2005), “Research on noise and vibration reduction at DB to improve the environmental friendliness of railway traffic”, *J. Sound Vib.*, **293**, 1058-1069. https://doi.org/10.1016/j.jsv.2005.08.065.

Shorter, P.J. and Langley, R.S. (2005), “Vibro-acoustic analysis of complex systems”, *J. Sound Vib.,* **288**(3), 669-699. https://doi.org/10.1016/j.jsv.2005.07.010.

Song, X., Li, Q. and Wu, D. (2018), “Prediction of Low-to-medium Frequency Structure-borne Noise Radiated from Rail Transit Concrete Bridges”, *J. China Railway Soc.*, **03**, 126-131. https://doi.org/10.3969/j.issn.1001-8360.2018.03.019.

Song, X., Wu, D. and Li, Q. (2015), “A 2.5-dimensional infinite element based method for the prediction of structure-borne low-frequency noise from concrete rail transit bridges”, *J. Vib. Eng.*, **6**, 929-936. https://doi.org/10.16385/j.cnki.issn.1004-4523.2015.06.010.

Song, X., Wu, D. and Li, Q. (2015), “A 2.5-dimensional infinite element based method for the prediction of structure-borne low-frequency noise from concrete rail transit bridges”, *J. Vib. Eng.*, **6**, 929-936. https://doi.org/10.16385/j.cnki.issn.1004-4523.2015.06.010.

Thompson, D. (2009), *Railway Noise and Vibration: Mechanisms, Modeling and Means of* Control, Elsevier, United Kingdom.

Wang X., Zhang, N. and Qi, S. (2014), “Study on vibration and noise radiation of urban rail transit bridge”, *Railway Construct.*, **2014**(1), 11-15. https://doi.org/10.3969/j.issn.1003-1995.2014.01.04.

Zhang, X. and Li, X. (2015), “Study on the effect of fastener stiffness and damping on vibration and noise of railway box girder”, *Vib. Shock.*, **15**, 150-155. https://doi.org/10.13465/j.cnki.jvs.2015.15.027.

Zhang, X., Zhang, J. and Li, X. (2015), “Beam plate hybrid element analysis of vibration and noise induced by bridge vehicle”, *Noise Vib. Control,* **35**(01), 89-92+109. https://doi.org/10.3969/j.issn.1006-1335.2015.01.018.

Zhang, X., Zhang, J. and Li, X. (2016), “Modified FE-SEA model to predict low frequency noise of box girders and test verification”, *J. Vib. Eng.,* **29**(02), 237-245. https://doi.org/10.16385/j.cnki.issn.1004-4523.2016.02.007.